frontiers | Frontiers in Materials

TYPE Original Research
PUBLISHED 28 October 2022
DOI 10.3389/fmats.2022.1005864

OPEN ACCESS

EDITED BY
Quoc Tri Phung,
Belgian Nuclear Research Centre, Belgium

REVIEWED BY
Afonso Azevedo,
State University of the North Fluminense Darcy Ribeiro, Brazil
David García,
Amphos 21, Spain
Didier Snoeck,
Université libre de Bruxelles, Belgium

*CORRESPONDENCE
Eros Mossini,
eros.mossini@polimi.it

SPECIALTY SECTION
This article was submitted to Structural Materials,
a section of the journal Frontiers in Materials

RECEIVED 28 July 2022
ACCEPTED 28 September 2022
PUBLISHED 28 October 2022

CITATION
Santi A, Mossini E, Magugliani G, Galluccio F, Macerata E, Lotti P, Gatta GD, Vadivel D, Dondi D, Cori D, Nonnet H and Mariani M (2022), Design of sustainable geopolymeric matrices for encapsulation of treated radioactive solid organic waste.
Front. Mater. 9:1005864.
doi: 10.3389/fmats.2022.1005864

Design of sustainable geopolymeric matrices for encapsulation of treated radioactive solid organic waste

Andrea Santi[1], Eros Mossini[1]*, Gabriele Magugliani[1], Francesco Galluccio[1], Elena Macerata[1], Paolo Lotti[2], Giacomo Diego Gatta[2], Dhanalakshmi Vadivel[3], Daniele Dondi[3], Davide Cori[4], Hélène Nonnet[5] and Mario Mariani[1]

[1]Laboratory of Radiochemistry and Radiation Chemistry, Department of Energy, Politecnico di Milano, Milan, Italy, [2]Department of Earth Sciences, University of Milan, Milan, Italy, [3]Department of Chemistry, University of Pavia, Pavia, Italy, [4]Laboratory of Processes Qualification, Nucleco S.p. A., Roma, Italy, [5]CEA, DES, ISEC, DE2D, Univ Montpellier, Marcoule, France

Among radioactive by-products generated by nuclear technologies, solid organic waste is drawing attention because of difficult management and incompatibility with the disposal strategies traditionally adopted. Recently, geopolymers have been proposed as valid and green alternatives to cement-based matrices. In this work, novel geopolymeric formulations have been studied at laboratory scale to encapsulate ashes from incineration of surrogate solid organic waste and to further pursue sustainability and circular economy goals. Indeed, the most widely used precursor of literature geopolymers, calcined kaolin, has been totally replaced by natural raw materials and recycled industrial by-products. In addition, a highly zeolitized volcanic tuff has been chosen to further improve the intrinsic cation-exchange capacity of the geopolymer, hence enhancing waste-matrix interaction. The alkaline activation of the precursors, achieved without silicates of any metal, resulted in a promisingly durable geopolymeric matrix, whose chemical composition has been optimised to provide compressive strength above 10 MPa after 28 days of curing. A water-saturated sealed chamber provided the optimal curing condition to limit the efflorescence and improve the mechanical

Abbreviations: AO, aluminium oxide; BFS, ground-granulated blast-furnace slag; CEA French Alternative Energies and Atomic Energy Commission; FA, fly ash; ICP-MS, inductively coupled plasma mass spectrometry; IRIS, Installation for Research on Incineration of Solids; KIPT, Kharkiv Institute of Physics and Technology; MK, metakaolin; PC, Portland cements; RSOW, radioactive solid organic waste; SH, sodium hydroxide; SW, surrogate waste; TGA, thermogravimetric analysis; VT, volcanic tuff; WAC, waste acceptance criteria; WTS, water-to-solid; XRD, X-ray powder diffraction.

properties. At least 20 wt% loading of treated surrogate waste was achieved, without compromising workability, setting time, and compressive strength, the latter remaining within acceptable values. In order to demonstrate matrix durability, leaching behaviour and thermal stability were preliminarily assessed by immersion tests and thermogravimetric analyses, respectively. The leachability indices of constituent elements resulted far above 6, which is the generally agreed requirement for cement-based matrices. Moreover, the mechanical resistance was not worsened by the water immersion. The preliminarily obtained results confirm the promising properties of the new matrix for the immobilization of nuclear waste.

KEYWORDS

nuclear waste management, radioactive solid organic waste, geopolymer, waste acceptance criteria, durability, sustainability, zeolitic tuff

Introduction

The brisk development of the global economy caused by industrialization, along with changing of lifestyle patterns, has led to a steep increase of energy consumption (Xie et al., 2018; Aydin, 2019). In order to satisfy such a growing demand, availability, cheapness, and distribution have become key aspects for the production of energy (Ismail et al., 2014; Gralla et al., 2017; Lopez-Solis and Franois, 2018). At the same time, concerns about resource availability, climate change, air quality, and supply-related security have arisen (Perera, 2018; Azam et al., 2021).

Among the countries exploiting nuclear sources to produce energy and for other technological purposes, there are some which do not generate significant quantities of radioactive waste to justify the implementation of national disposal protocols at research and industrial levels. Alternatively, it may happen, even in countries producing large quantities of radioactive waste, that some by-products are generated in small amounts, and research efforts have never addressed the problem of their management. However, it may happen as well that certain subclasses of radioactive waste, despite being generated in large quantities, are particularly difficult to handle due to specific properties such as chemical and physical instabilities, or toxicity- and safety-inherent hazards (Zhang et al., 2009; Martinez, 2022). Waste falling into this category suffers from a lack of knowledge. As a result, the common strategy so far has been to store this waste waiting for the radionuclides to decay or for other countries to develop and operate a valid disposal solution (International Atomic Energy Agency, 2008). However, their accumulation has recently reached alarming levels and attracted the attention of the scientific community, which refers to them as *challenging* radioactive waste (International Atomic Energy Agency, 2007). This category includes radioactive solid organic waste (RSOW), which is object of scientific research within the H2020-PREDIS project (European Commission, 2022).

In the past, several techniques for immobilization of RSOW were studied, and nowadays some of them are still used. Each of these is characterized by downsides which are too critical to be ignored. For instance, direct encapsulation in Portland cements (PC) may show low loading factors and unsatisfactory durability, while bituminization involves the use of flammable materials (Zakharova and Masanov, 2000; Pan et al., 2009). Furthermore, waste-related issues, namely swelling and flammability, related to the organic content of the waste, dispersivity and potential radionuclides leachability, have hindered, so far, the development of a proper matrix for direct confinement (Wang and Wan, 2015). In the recent years, however, encapsulation in geopolymers, introduced by Davidovits in the late '70s, emerged as a promising alternative to PC (Davidovits, 1991). This class of alkali-activated aluminosilicate materials has received considerable attention because of their low cost, excellent mechanical, thermal, and chemical stability, low energy consumption, and reduced emissions of greenhouse gases at the production cycle, characteristics which place them in a category of new environmentally sustainable materials (Duxson et al., 2005; Duxson et al., 2007; Rashad and Zeedan, 2011). In addition, to further improve the disposability of RSOW, pre-treatment operations (e.g., pyrolysis/calcination, wet oxidation, molten salt baths) are commonly addressed to stabilise and reduce the volumes of waste by removing the organic content (Dubois et al., 1995; Castro et al., 2017; Scheithauer et al., 2017).

Geopolymers are generally synthesized close to room temperature by reaction of an aluminosilicate binder with a concentrated alkali metal silicate and/or hydroxide solution (Yao et al., 2009; Chi, 2012; Provis et al., 2015). The alkaline environment promotes the dissolution of Si^{4+} and Al^{3+} species from the amorphous phase of the solid precursors, which condensate afterwards into a coagulating gel forming a tetrahedral network of silicates and aluminates (Rattanasak and Chindaprasirt, 2009; Deir et al., 2014). The product of this reaction is a sodium alumino-silicate hydrate gel, generally

referred to as N-A-S-(H), where N stands for Na_2O, A for Al_2O_3, S for SiO_2, and H, written in brackets, for water, as it does not constitute a major structural component (Provis and Bernal, 2014). The substitution of $Si(OH)_4$ by tetrahedral $Al(OH)_4^-$ in the network generates a negative charge which is balanced by the alkali cations provided by the activation solution (de Oliveira et al., 2022). Similarly, contaminant cations could neutralize the charge, thus establishing a strong interaction with the matrix (Niu et al., 2022). This interesting feature has promoted the application of geopolymers to the confinement of nuclear waste (Lee et al., 2019; Fan, 2020; Reeb et al., 2021).

Suitable precursors for geopolymerization reactions are naturally available pozzolanic materials, such as the highly reactive metakaolin (MK), prepared from kaolinite clays through energy-intensive calcination at around 700–800°C (Davidovits, 2018; Geddes et al., 2018). In several works, volcanic tuff has been proposed as more easily available and sustainable natural raw material (Haddad and Alshbuol, 2016; Ekinci et al., 2019; Kantarci et al., 2019). Moreover, in order to improve the environmental and economic sustainability and foster circular economy goals, the use of industrial by-products endowed with satisfactory pozzolanic and cementitious properties has been investigated (Parthiban et al., 2019; Podolsky et al., 2021). A wide range of recycling opportunities have been suggested: fly ash (FA) coming from coal burning in thermal power plants, ground-granulated blast-furnace slag (BFS), a by-product of iron and steel industries, red mud deriving from the extraction of alumina from bauxite, mine tailings, municipal waste ash, and food industry by-products such as palm oil and rice husk ashes (Diaz et al., 2010; Phoo-ngernkham et al., 2015; Parthiban et al., 2019; Qaidi et al., 2022a; Qaidi et al., 2022b). Recycling of industrial by-products as geopolymeric precursors is a sustainable alternative to MK-based geopolymerisation and cementation, as it contributes to mitigate environmental footprint and associated costs. A further advantage, especially for FA, is the elimination of health and environmental hazards originating from the storage of such toxic material (Assi et al., 2018; Assi et al., 2020). Regarding the main drawbacks, the robustness of the formulation towards regional availability and intrinsic composition variability of the precursors is a factor that may affect not only the lifecycle assessment of the geopolymer, but its performance as well (Provis and Bernal, 2014). Moreover, the moderate cost, insufficient global production and stockpile of alkali metal hydroxide and silicate make the activation solution supply the limiting factor for large scale implementation of geopolymers (Provis and Bernal, 2014; Assi et al., 2020; de Oliveira et al., 2022).

The development of a durable geopolymeric matrix capable of encapsulating RSOW ashes is the main objective of this work. Moreover, efforts have been focused to overcome the aforementioned issues and pursue sustainability and circular economy goals, ensuring lower cost and satisfactory worldwide availability of raw materials. To do so, sodium hydroxide (SH) has been picked over potassium hydroxide and alkali silicates for activation purposes, while MK has been replaced by more sustainable geopolymer precursors: highly zeolitized volcanic tuff (VT), along with industrial by-products, such as FA and BFS. Specifically, the high zeolitic content of the VT has been the main reason behind its choice. In fact, the intrinsic cation exchange capacity of geopolymers could be further improved by the addition of zeolites, with a view toward enhancing waste-matrix interaction (El-Eswed et al., 2015; Siyal et al., 2018; Niu et al., 2022). Chabazite is the most abundant zeolite in the employed VT. Its use has already been suggested to selectively bind Cs^+, which is one of the most difficult ions to be confined (Dyer and Zubair, 1998; Baek et al., 2018). Different formulations of this novel matrix have been investigated at laboratory scale as more economically and environmentally sustainable processes for the conditioning of treated RSOW. The matrices were microscopically and macroscopically characterised by means of X-ray powder diffraction (XRD), thermogravimetric analysis (TGA), compression and immersion testing. Compliance with waste acceptance criteria (WAC) was assessed by comparison with reference values for low- and intermediate-level cemented waste. As treated surrogate waste (SW), the ashes coming from Installation for Research on Incineration of Solids (IRIS) were considered. Such pilot plant, developed at French Alternative Energies and Atomic Energy Commission (CEA) Marcoule for research and development support, is devoted to the treatment of the RSOW contaminated by α-emitting actinides from glove boxes employed in the nuclear industry (Lemont, 2012; Fournier et al., 2020). The IRIS plant exclusively works with radiologically-inactive surrogate waste, and the ashes are produced by the co-incineration of a mixture of different organic solids, representative of glove box waste from a mixed oxide fuel production facility and composed of polyvinyl chloride, latex, neoprene, ethylene-vinyl acetate, cotton and Kleenex®, and anionic ion-exchange resins, as reported by Lemont (Lemont, 2012). Additions of CeO_2 to the waste mixture could be considered to simulate plutonium behaviour. The multi-step process, thoroughly described elsewhere (Lemont, 2012), is implemented in rotating kilns: an oxidative pyrolysis at 550°C produces a pitch, which is processed afterwards in a calcining step at 900°C in oxygen-enriched atmosphere. Overall, a volume reduction of the waste of about a factor 30 is achieved, and the inactive surrogate ashes arising from the process are comprised of a material rich in calcium, zinc, and aluminosilicates, with

negligible levels of residual carbon, which makes such ashes ideal candidates for the encapsulation in geopolymeric matrices (Wang and Wan, 2015; Lee et al., 2019).

Materials and methods

Precursors and additives

The main precursor for geopolymerization is the VT (Zeolite Fertenia™), while additions of FA and BFS, kindly provided by the Kharkiv Institute of Physics and Technology (KIPT), were employed as well, without further processing. The FA comes from the thermal power station in Burshtym, Ukraine, while the BFS is produced by the Cembudservice Company in Kiev, Ukraine. The inorganic ashes encapsulated as SW come from the IRIS pilot plant managed by the CEA. Such residues, having apparent density of 0.2 g/cm^3 and particle size distribution mainly centred between 0.1 and 1 mm, were preliminary blended with a Moulinex MC300132 grinder to break the agglomerates and obtain a finer powder, homogeneous to naked eye. The chemical compositions of these materials are reported in **Table 1**, and their fineness was investigated. Geopolymeric grouts were enriched in aluminium oxide (AO) (MERCK) and activated with SH (Sigma-Aldrich). Both these reagents were of analytical grade. SH pellets were quickly ground with mortar and pestle to obtain a fine powder with a grain size closer to that of the precursors, and then stored in an airtight container to avoid carbonation. For dilutions of aqueous samples undergoing inductively coupled plasma mass spectrometry (ICP-MS) analyses, ultrapure water (Milli-Q gradient from MilliporeSigma) and 65 wt% ultrapure HNO_3 (Sigma-Aldrich) were used.

Instrumentation

XRD patterns were collected with an automated Panalytical X'Pert Pro modular diffractometer, equipped with a X'Celerator detector. Operating conditions were: monochromatised Cu-Kα radiation, 40 kV, 40 mA, 2θ range from 4 to 80° and step size of 0.017°, counting time of 240 s per step, side-loaded samples. Phase identification was performed using the X'pert HighScore software and database. Obtained patterns were processed and plotted using MATLAB software. TGAs were performed using a Mettler Toledo TGA1 STAR^e thermogravimetric analyser, heating the samples with a rate of 10 °C/min, under air atmosphere (mass flow: 100 ml/min), from 25 to 800°C. Samples for this analysis, 5 mg sized, were prepared by grinding hardened specimens down to sub-millimetric powders. Obtained data were extracted and processed using MATLAB software. Element determination was performed with a PerkinElmer NexION 2000 inductively coupled plasma mass spectrometer, with calibration curves obtained with Inorganic Ventures CMS-x standards duly diluted with ultrapure 1 wt% nitric acid. The samples were prepared for ICP-MS analysis by diluting the starting aqueous solutions with ultrapure 1 wt% nitric acid. Compression tests were carried out according to BS EN 12390-3:2019 standard (British Standards Institution, 2019a), and the reference value for the purposes of this work was set at 5 MPa (28 days) in agreement with Italian guidelines (Istituto Superiore per la Protezione e la Ricerca Ambientale, 1987; Ente Nazionale Italiano di Unificazione, 2006). Specimens underwent compression by gradually increasing the load applied by the platens of a C089PN591 Matest compression-testing machine. Compressive strength values were derived by dividing the maximum load by the cross section of the specimens. Workability was measured with a RMU Flow Table in agreement with BS EN 12350-5:2019 standard (British Standards Institution, 2019b), while the setting time was derived with a VICAMATIC-2 Automatic Setting Time Tester according to BS EN 196-3:2016 standard (British Standards Institution, 2016).

Geopolymeric matrices

Precursors and additives were combined according to the solid activation method represented in **Figure 1**. Weighed amounts of VT, FA, BFS, AO, SH, and SW (when included) were added to a vessel and homogenised. The right amount of water was subsequently poured, and the mixing started right afterwards. This procedure, which does not involve the preparation of an activation solution as is most often done (Chi, 2012; Ji and Pei, 2019), was developed to simplify the production process ahead of industrial implementations, reducing the number of preparation steps and, consequently, the complexity of the required machinery.

Mixing of the fresh grouts was carried out using a Kenwood KM280 stand mixer at mid-low speed until complete homogenisation of the paste. Under this condition, it was found that 10 min were enough, so this time has been taken as a reference for the preparation of all the samples. The compositions of the formulations are reported in **Table 2**. The water-to-solid (WTS) ratio is computed by dividing the total water mass, both structurally-incorporated and added, by the total mass of the dehydrated solid powders.

Formulation A and A-bis differ for the external addition of AO, while formulations B and B-bis were designed with different WTS ratios in order to investigate the effect of this parameter. Formulations C-10 and C-20 are obtained from formulation C—using its relative proportion between VT, FA, and BFS—by replacing 10 wt% and 20 wt% of the sample with the SW, respectively. According to precursors elemental compositions (**Table 1**), the amount of AO has been duly

TABLE 1 Chemical composition of the materials used in the geopolymeric matrices, as provided by the suppliers.

Precursor	Composition [wt%]								
	SiO_2	Na_2O	K_2O	Al_2O_3	CaO	MgO	Fe_2O_3	TiO_2	H_2O
Volcanic tuff	52.09	0.51	6.08	17.13	5.77	1.94	3.69	0.52	7.98
Fly ash	46.12	1.17	0.93	18.00	4.09	1.46	22.17	1.78	0.60
Blast-furnace slag	40.14	0.42	0.40	6.02	45.10	5.07	0.62	0.29	0.00
Surrogate waste	29.35	0.95	3.61	28.46	13.55	4.53	0.63	0.69	0.00

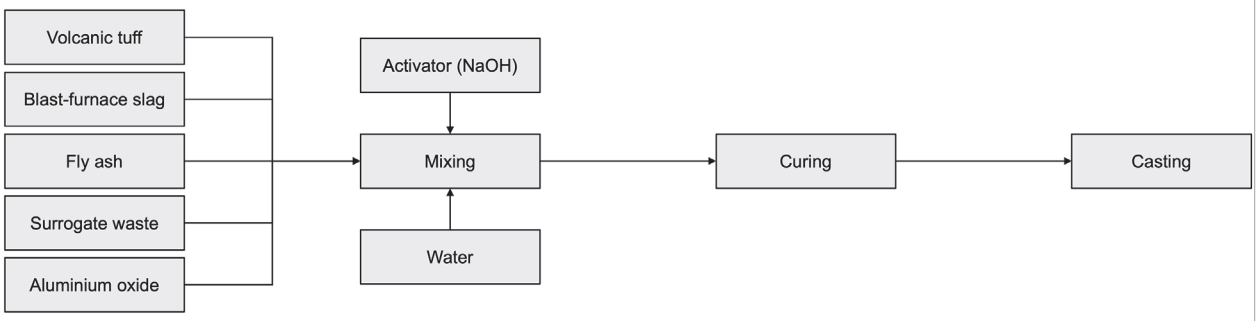

FIGURE 1
Geopolymer mixing: weighing of the powders; addition of the sodium hydroxide; addition of the water; start of mixing; homogenization of the mixture; geopolymer paste.

TABLE 2 Overall chemical composition of the geopolymeric formulations and the contents of raw materials.

Formulation	Raw materials [wt%]						WTS	Chemical composition [wt%]				
	VT	FA	BFS	SW	AO	SH	[kg/kg]	SiO_2	Al_2O_3	Na_2O	CaO	H_2O
A	34.2	16.3	14.1	0.0	1.0	10.2	0.35	31.0	10.6	8.6	9.0	28.9
A-bis	34.6	16.4	14.3	0.0	0.0	10.3	0.36	31.3	9.7	8.6	9.1	29.2
B	25.5	19.6	19.5	0.0	1.0	10.2	0.35	30.2	10.1	8.5	11.1	28.1
B-bis	24.7	19.0	19.0	0.0	1.0	9.8	0.40	29.2	9.7	8.2	10.8	30.5
C	14.7	24.1	24.1	0.0	2.0	8.1	0.40	28.5	10.3	6.9	12.7	29.7
C-10	12.0	20.0	20.0	10.0	2.6	7.1	0.42	26.5	12.3	6.1	11.9	30.5
C-20	8.8	14.4	14.4	20.0	6.1	6.7	0.43	22.8	16.7	5.8	10.3	31.7
D	0.0	32.2	29.3	0.0	2.7	9.0	0.40	26.6	10.3	7.6	14.5	28.6

adjusted to ensure the same SiO_2 and Al_2O_3 concentration in the resulting grout. Similarly, the water amount has been slightly increased along with waste loading to guarantee similar workability of formulation C. Overall, the content of VT decreases from formulations A to D, while that of FA and BFS increases. Eventually, formulation D was designed with chemical composition similar to the others, but without the VT.

Once mixed, the grouts were poured into equilateral cylindrical moulds with dimension of 5 cm and vibrated with a hard-rubber tamper for 2 min to reduce air bubbles inclusions and flatten the upper surface. Three curing periods were investigated: 10, 14, and 28 days. Moreover, four different curing configurations were tested: 1) in-mould; 2) open container; 3) sealed container; 4) water-saturated sealed container. The latter configuration was achieved by placing a lifted disk in the sealed beaker on which the monolith is laid, and by pouring a small volume of de-ionized water on the bottom, without wetting the specimens. If not explicitly stated, the curing period was set to 28 days. Afterwards, the monoliths were retrieved and tested.

Leaching and water immersion

Preliminary evidence of geopolymers leachability and stability towards immersion were obtained by means of leaching experiments and post-immersion mechanical testing. The former was performed in agreement with ANSI/ANS-16.1-2003 protocol (American Nuclear Society, 2003), and the leachability

indices of the main matrix constituents (i.e., silicon, aluminium, sodium, and calcium) were accordingly derived. To do so, a set of capped jars was suitably washed and filled with the amount of ultrapure water imposed by the protocol. Given the preliminary nature of the investigation, only ultrapure water was used as leachant. Geopolymeric specimens, in-mould cured for 48 h and subsequently stored in water-saturated sealed containers until completion of 28 days of curing, were immersed wetting the whole surface. In order to monitor the release of the species over time, leachants were periodically renewed at 2, 6, 30, 78, and 174 h, for a total experiment duration of two weeks (342 h). Leachates were tested with pH-indicator paper and then diluted with 0.14 M ultrapure nitric acid and analysed *via* ICP-MS. Downstream of water immersion, geopolymeric specimens underwent compression test. To provide reference values, corresponding monoliths of identical composition were prepared as blank samples. These were cured in moulds for 48 h and in water-saturated sealed containers for the subsequent 40 days, 26 for the completion of curing stage and 14 for the duration of the leaching experiment, in order to reach the same overall curing time.

Results and discussion

Grain size and mineralogical nature of the sample

Figure 2 shows some selected microphotographs of the precursor powders, obtained by optical microscopy. The VT consists of a fine powder made by grains usually smaller than 5–10 μm. FA is less homogeneous and consists of sub-millimetric to micrometric grains. The larger particles could be aggregates of finer grains, partly cemented. In particular, spherical grains (glass), mostly smaller than 200 μm in size, are observed. For BFS, more than 70% of the grains are sub-micrometric, about 30% are on the order of a few micrometres in size (below 5 μm), and only a very low fraction of individuals of about 10 μm is observed. The ground SW is mainly composed of two parts:

- a very fine, white-coloured material, with sub-micrometric grains, often coalesced to give aggregates of a few hundred μm;
- a coarser material, sub-millimetric in size, mostly covered by the fine white material and therefore not always immediately identifiable.

On the other side, AO presents a uniform grading. The maximum size of the sub-spherical grains does not exceed 200 μm.

Some representative X-ray diffraction patterns of solid precursors and hardened geopolymeric samples obtained in this study are shown in **Figure 3**. The X-ray diffraction data confirm the mineralogical composition of the VT provided by the supplier: chabazite zeolite (ideally $|(Ca_{0.5},K,Na)_x(H_2O)_{12}|\ [Al_xSi_{12-x}O_{24}]$, around 65 wt%), phillipsite zeolite (ideally $|\ (Na,K,Ca_{0.5})_x\ (H_2O)_{12}|\ [Al_xSi_{16-x}O_{32}]$, around 5 wt%), K-feldspar (ideally $(K,Na)AlSi_3O_8$, around 4 wt%), biotite (ideally $K(Mg,Fe)_3AlSi_3O_{10}(OH)_2$, around 2 wt%), diopside pyroxene (ideally $CaMgSi_2O_6$, around 4 wt%), glass (around 20 wt%). The FA is mainly amorphous, along with a low fraction of quartz (SiO_2) and mullite ($Al_{4+2x}Si_{2-2x}O_{10-x}$). The diffraction pattern of the BFS confirms its essentially amorphous nature, and the minor diffraction peaks can be ascribed to åkermanite (ideally $Ca_2Mg(Si_2O_7)$) and, likely, to calcite ($CaCO_3$, by late carbonation). The SW shows a complex phase composition: there is a high amorphous fraction, along with chlorapatite (ideally $Ca_5(PO_4)_3Cl$, dominant), diopside pyroxene (dominant), anhydrite (ideally $CaSO_4$), spinel (ideally $MgAl_2O_4$), plagioclase (ideally $(Na,Ca)[(Si,Al)AlSi_2]O_8$), and quartz. The broad peaks characteristic of the AO suggest its microcrystallinity and the predominance of δ-alumina, while α-alumina and $Al(OH)_3$ are also observed as subordinate phases.

The diffraction patterns of the hardened geopolymeric samples obtained by formulations B, B-bis, C, and C-10 are mutually similar, and reflect the mineralogical composition of the parental precursors: a high fraction of amorphous matrix, as shown by the background profile, along with chabazite (dominant), phillipsite, quartz, and plagioclase. Different is the phase composition of the samples obtained by formulation C-20, where the amorphous fraction is dominant, along with chabazite, chlorapatite, diopside, quartz, and plagioclase. A few additional weak Bragg diffraction peaks are observed, but not unambiguously ascribable to a hydrous sulphates (like $Na_{12}Mg_7(SO_4)_{13}{\cdot}15H_2O$) or to a hydrous phosphate (like $Na_{3.2}PO_4Cl_{0.2}{\cdot}11H_2O$).

The amorphous content in the resulting geopolymer indicates that the alkalinity of the activating media promoted the dissolution of aluminosilicate species from the precursors and induced their subsequent crosslinking (Nath et al., 2017). The same occurs for AO, whose Al_2O_3- and $Al(OH)_3$-related Bragg peaks are not observed in the hardened geopolymers, and, thus, disappear during the geopolymerization reaction. On the other hand, chabazite, phillipsite, chlorapatite, quartz, and plagioclase, coming from the parental VT, do not dissolve and remain embedded in the matrices. In fact, the alkaline activator is known to preferentially react with the amorphous phase of the precursors rather than with the crystalline phases (Rattanasak and Chindaprasirt, 2009; Djobo et al., 2014; Firdous et al., 2018). Thus, these mineralogical species can provide waste-matrix interactions *via* cation-exchange processes, as described in literature (Colella, 1996; Dyer and Zubair, 1998; Cappelletti et al., 2011).

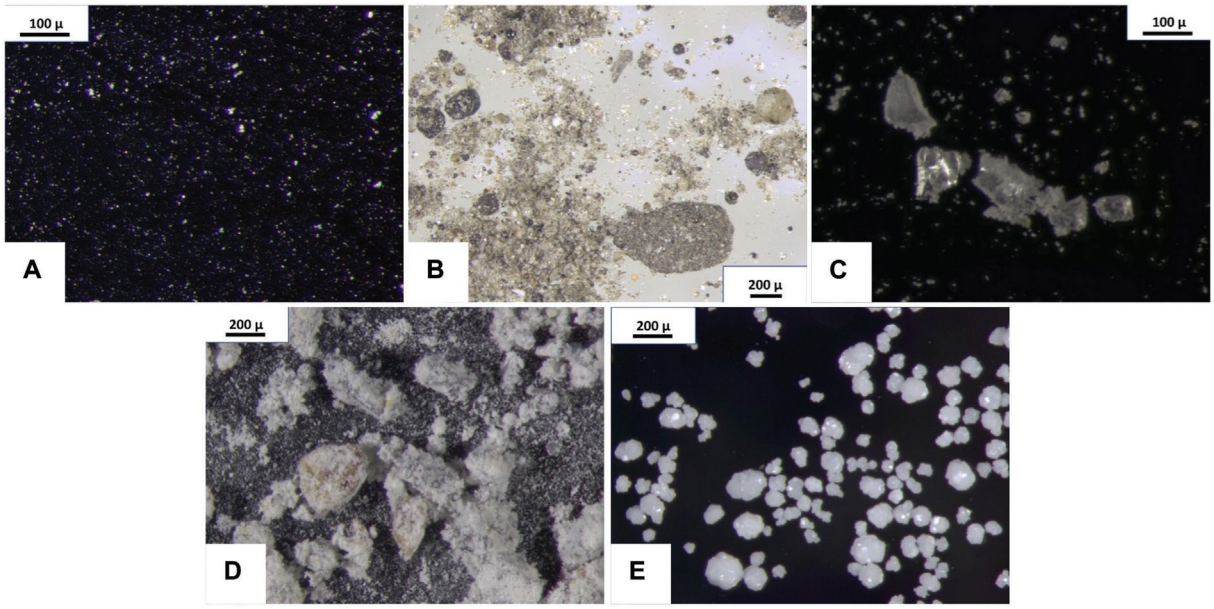

FIGURE 2
Microphotographs of the geopolymeric precursors: **(A)** volcanic tuff; **(B)** fly ash; **(C)** blast-furnace slag; **(D)** surrogate waste; **(E)** aluminium oxide.

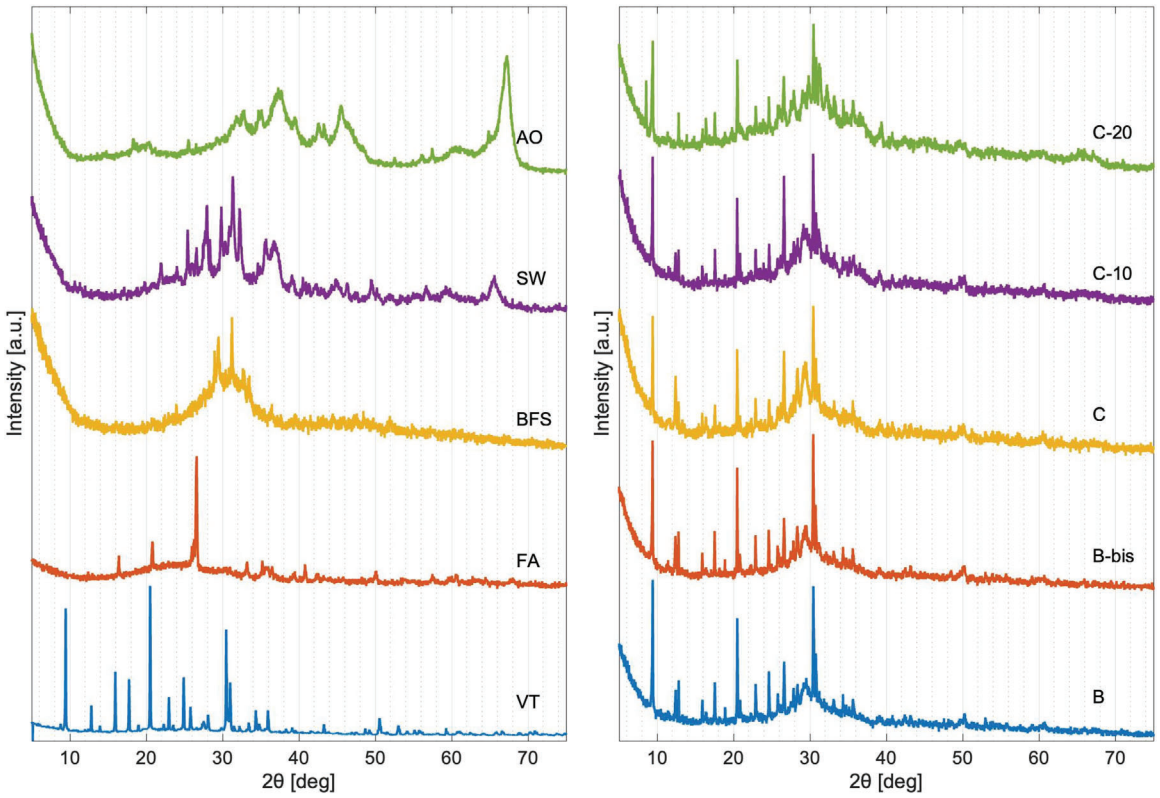

FIGURE 3
Diffraction patterns of precursors (left) and geopolymeric matrices (right).

Thermogravimetric analyses

The thermal properties of the hardened geopolymeric samples were investigated by means of TGA. This analytical technique may provide insight about the degree of geopolymerization (Firdous et al., 2018). Samples were previously ground to sub-millimetric powders, and their thermal decomposition was analysed, in terms of weight loss, as a function of temperature (Douiri et al., 2016). In the current objective of geopolymers, materials were tested up to 800 °C. Water molecules, free or embedded within the matrix, could be the main reasons for changes in the mechanical characteristics (Fang and Kayali, 2013). More in detail, there are three ways of water presence in the matrices: free molecules physically absorbed in the network, molecules in the gel pores of the matrices, and a chemically combined structural hydroxyl group from water molecules (Fang and Kayali, 2013). In **Figure 4**, losses of about 25 wt% close to 105 °C are observed. This is due to free or interstitial water (Bagheri et al., 2018; Firdous et al., 2018). Usually, in the case of traditional geopolymers, weight losses from 150 to 600 °C are related to the release of structural water and hydroxyl groups, for example Si-OH and Al-OH (Aliabdo et al., 2016; Firdous et al., 2018). The degree of geopolymerization could be estimated from this stage, since structural water is originated during the condensation of the aluminate and silicate species to form the N-A-S-(H) gel (Weng and Sagoe-Crentsil, 2007; Djobo et al., 2016a). Unfortunately, the high amount of calcium in BFS precursor complicates the interpretation of the results, since Ca-containing phases dehydrate below 250 °C (Bernal et al., 2011). The release of structural water is less than 5% of the total mass, although in agreement with the literature (Djobo et al., 2016a; Firdous et al., 2018). This is more evident in formulations C-10 and C-20, probably due to the non-negligible content of calcium in the SW. The carbonate decomposition starts above 600 °C. Its presence in the matrix is mainly due to unreacted NaOH and $Ca(OH)_2$ precipitated due to the high basicity of the activation solution (Provis and Bernal, 2014; Baykara et al., 2017). Even if this mass loss is rather low (less than 5%) with respect to the total mass, it suggests that the amount of alkaline activator in the formulation should be reduced.

Macroscopic characterisation

Density, workability and setting time of B, C, and C-20 grouts were measured to derive information about some practical properties of the fresh pastes. The obtained results are reported in **Table 3**. The comparison between formulations B and C allows to highlight the effects of WTS ratio and amount of BFS and FA. In fact, as the WTS ratio and amount of FA increase, it was noted that the workability significantly improves (Nath and Sarker, 2014). This result is important, since it is known that workability worsens when the BFS content is increased (Nath and Sarker, 2014; Xie et al., 2019). In fact, the use of mainly smooth, spherical, and finer-size FA grains positively affects the workability, rather than the coarser-shaped BFS (Podolsky et al., 2021). Moreover, moving from formulations B to C, increasing amounts of FA and BFS partially replace VT, thus the reactivity of the mixture increases as well and, consequently, the setting time shortens (Chindraprasirt et al., 2009; Rattanasak and Chindaprasirt, 2009). This result is coherent with the literature and with XRD findings of this work, for the highly crystalline VT material is endowed with lower pozzolanic reactivity compared to the prevalently amorphous FA and BFS precursors (Rattanasak and Chindaprasirt, 2009; Firdous et al., 2018). Moreover, by increasing the amount of BFS, Ca content increases as well. This further contributes to reducing the setting time (Provis and Bernal, 2014). To avoid excessively fast setting at high BFS contents, the WTS ratio needs to be increased (Kumar et al., 2010; Xie et al., 2019). The particle size of the precursors is another parameter which influences the setting time. Indeed, the finer the materials, the greater the reactivity (Djobo et al., 2016b). For this reason, the grain size of all solid constituents was checked to be at least sub-millimetric and, in case of SW, grinding was performed prior to use. Thanks to the adjusted water content, the addition of SW in formulation C-20 does not compromise the grout workability, but the excess water acts as a retardant, increasing the setting time by more than six times (Cantarel et al., 2015). Overall, the values shown in the table are consistent with applicability in industrial settings, for technological scale-up. Furthermore, the evidence of these preliminary tests suggests that, by duly tuning WTS ratio, BFS and FA amounts in the formulation, optimal values of workability and setting time may be obtained, depending on the requirements of specific applications.

Upon hardening, cast specimens resembled the one shown in **Figure 5**. By visual inspection, some apparent defects were highlighted. Besides a non-perfectly flat upper surface, some cavities with maximum width of 3 mm were noticeable in the upper volume of the specimen, while some smaller and more sporadic pores are visible in the lower half. Such pore distribution suggests that vibration should be improved. In fact, it was just long enough to bring those bubbles from bottom to top, but without completing the ascent to the surface. The presence of smaller pores at the bottom, on the other hand, suggests that the intensity of vibration was not sufficient as well. The presence of cavities has consequences on the mechanical and lixiviation properties of the material (Rickard et al., 2013; Hajimohammadi et al., 2019; Walbrück et al., 2020).

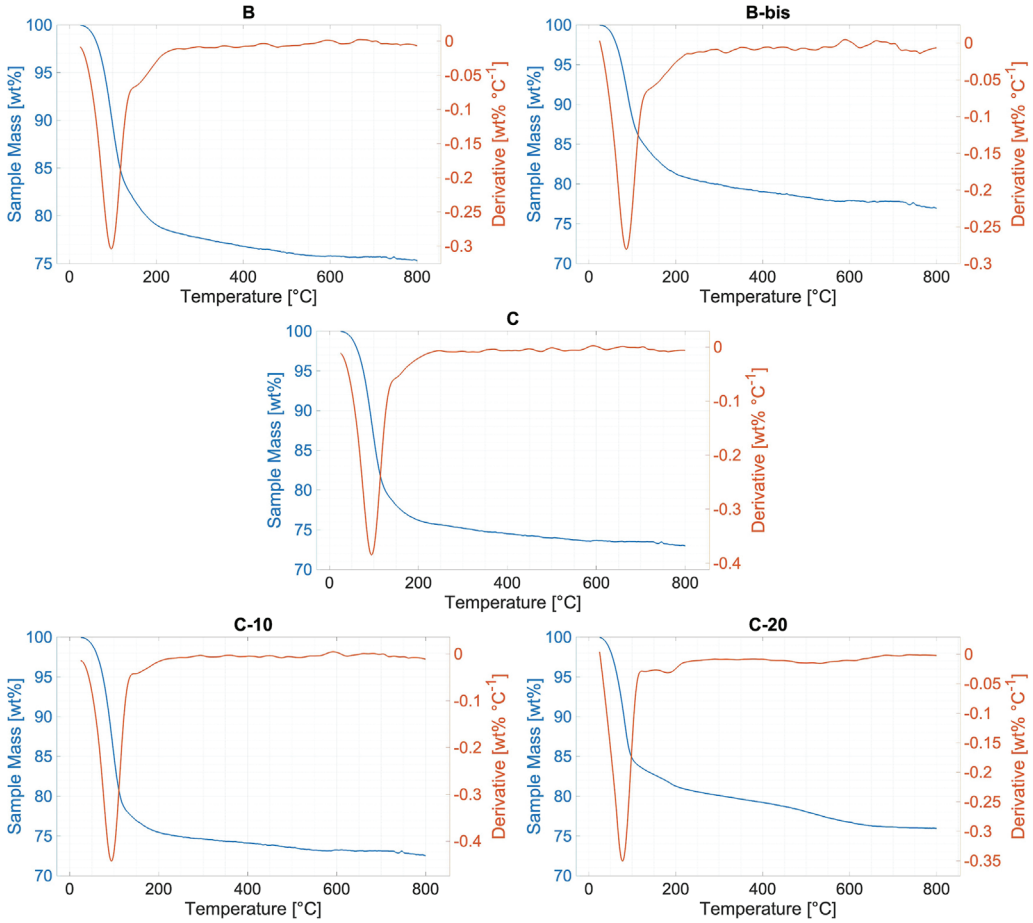

FIGURE 4
Thermogravimetric results.

TABLE 3 Density, workability and setting time data.

Formulation	Density [g cm^{-3}]	Workability [%]	Setting - beginning [h]	Setting - end [h]
B	2.15 ± 0.05	30 ± 5	0.83 ± 0.08	3.00 ± 0.08
C	2.11 ± 0.04	50 ± 5	0.67 ± 0.08	1.17 ± 0.08
C-20	1.98 ± 0.08	60 ± 5	4.08 ± 0.08	7.33 ± 0.08

Mechanical properties

The geopolymeric formulations were tested to determine their compressive strengths after proper smoothing of the upper face. In fact, the conditioning matrix must be resistant to the mechanical stresses that could arise due to normal operations and accidental conditions, such as waste handling, transport, and piling during storage and disposal (International Atomic Energy Agency, 1996). Some preliminary results have been obtained after 10 days of in-mould curing in order to shine a light on some important properties, such as WTS ratio and Al_2O_3 content in the formulation. On the other hand, the effects of curing temperature, different grain size of the precursors and concentration of the activator have not been investigated in this work. In fact, it is known that the use of higher curing temperature, finer materials, and higher activator concentration favour the dissolution of aluminium and silicon, generally resulting in an improvement of the mechanical properties (Bondar et al., 2011; Djobo et al., 2016b). Data are reported in **Figure 6**. It should be noted that the inhomogeneities (e.g., the cavities) certainly affect the mechanical properties and increase the experimental uncertainty, especially for such small-dimensioned samples. Moreover, only preliminary information can be obtained from these data, since curing is expected

FIGURE 5
Example of hardened geopolymeric monolith.

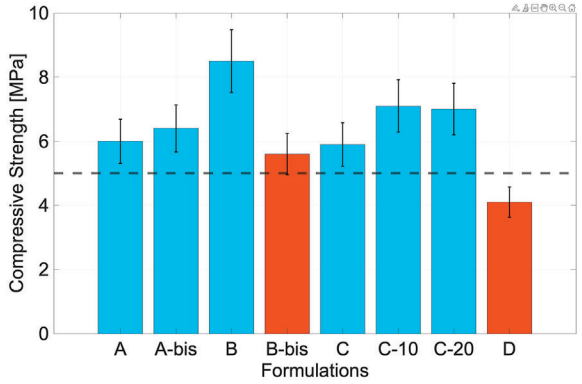

FIGURE 6
Compressive strength of the geopolymer formulations after 10 days of in-mould curing. The dotted line represents the minimum value imposed by the WAC for cement-based matrices.

to last for several weeks, even beyond the reference 28 days (Ge et al., 2018). In terms of compressive resistance, formulation B seems to be the most performant one. It should be noted as well that the introduction of a higher percentage of FA and BFS in formulation B with respect to A resulted in a significant increase, of about 30%, in compressive strength. This trend is coherent with the literature and the higher reactivity evidenced by setting-time experiments at increasing FA and BFS (Li and Liu, 2007; Kumar et al., 2010; Provis and Bernal, 2014). The compressive strength then decreases when VT is absent in formulation D. The absence of alumina in formulation A-bis seems not to significantly affect the compressive strength, at least after 10 days of curing, as the difference in performance between A and A-bis is within the uncertainties. This apparently unexpected result could be explained by reasonably assuming the curing was incomplete (Kouamo et al., 2012). The prediction of WTS ratio influence on compressive strength is also complicated at first sight. While a higher value of this property should guarantee better workability of the grouts and, thus, easier elimination of cavities during tamping of the moulds, an excess of water in the fresh grouts could decrease the reactivity of the geopolymer gel (El Idrissi et al., 2018). This hardly predictable behaviour is partially confirmed by data in **Table 2** and **Figure 6**. The comparison between B and B-bis suggests that the compressive strength decreases by increasing the WTS ratio from 0.35 to 0.40. This outcome may suggest that the presence of inhomogeneities (millimetric and sub-millimetric size) has a limited effect on the mechanical properties, that are more affected by the excess of water in the formulation, in agreement with the literature (Provis and Bernal, 2014; de Oliveira et al., 2022).

The results of the compression tests after 10, 14, and 28 days of curing for the A, A-bis and B formulations are shown in **Figure 7** (left). It is immediately noticeable that compressive strength non-linearly increases with the curing time (Mozumder et al., 2017; Ge et al., 2018). Most of the compressive strength was developed within the first few days of curing, with slower hardening afterwards. This suggests that the reactivity of the fresh grout is proportional to the concentration of the aluminosilicate species. Thus, the hardening occurs faster in the first few days, then it slows down asymptotically. The smallest increase after 28 days is achieved by formulation A-bis. This makes evident the effect of additional alumina: the unbalanced Si/Al ratio in formulation A-bis worsens the mechanical properties of the matrix (Davidovits, 1991; Kouamo et al., 2012). Furthermore, it is just as easily derived that the increased content of FA and BFS in formulation B with respect to A also contributes to the improved mechanical properties in the long term. This could be associated to the amorphous phases in the BFS, which are more easily dissolved than the crystalline phases of VT by the alkaline environment during the activation of the precursor powders (Deir et al., 2014). It is known that, under optimal conditions, a synergistic effect may be established by the concurrent use of Ca-rich and Ca-free precursors, BFS, FA and VT, respectively, to produce co-existing C-A-S-H and N-A-S-H gel phases after geopolymerization (Yip et al., 2005; Luhar and Luhar, 2022). Although the high basicity of the employed activation solution is expected to cause just partial C-A-S-H gel formation and non-negligible Ca precipitation as portlandite [namely $Ca(OH)_2$], the improvement of mechanical properties with increasing FA and BFS amounts is evident (Kumar et al., 2010; Provis and Bernal, 2014).

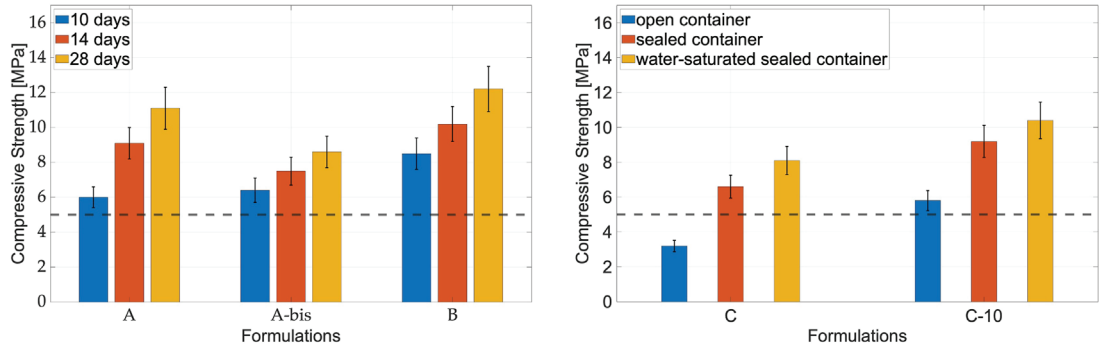

FIGURE 7
Compressive strength of the geopolymer formulations: (left) after 10, 14, and 28 days of in-mould curing; (right) after 10 days of curing in different conditions. The dotted line represents the minimum requirement imposed by the WAC for cement-based matrices.

A parallel study was carried out on formulations C and C-10 to optimise curing conditions. Three samples for each of the formulations were prepared, allowed to set in the mould, and removed after three days to perform curing in three different environments: open air, sealed, and water-saturated sealed container. Important effects on both mechanical strength and appearance of the specimens were observed. **Figure 8** shows three samples of formulation C, exposed to different curing environments. As it can be noted by visual inspection, a white solid polycrystalline material grows on the surface of the sample exposed to air (**Figure 8** (left)) (Ye and Radliska, 2017). Such a material has been identified through XRD as consisting of carbonates (nominally $CaCO_3$, $Na_2CO_3{\cdot}H_2O$ and $Na_3H(CO_3)_2{\cdot}2H_2O$). The diffraction pattern is shown in **Figure 9**. Surface carbonation occurs according to the following reaction (Pasupathy et al., 2016):

$$2\,OH^-_{(GP)} + CO_{2(G)} \rightleftharpoons CO^{2-}_{3\,(S)} + H_2O_{(L)} \qquad (1)$$

where "GP", "G", "L", and "S" stand for the geopolymeric, gaseous, liquid, and solid phases, respectively. On the contrary, the sample cured in sealed environment, shown in **Figure 8** (centre), exhibits a barely perceptible carbonate coating. In this case, the carbonation process was inhibited due to the limited amount of atmospheric CO_2 present in the closed container. Surface carbonation may be related to an excess of SH in the activation solution. Indeed, unreacted hydroxyl ions are mobile within the porous geopolymer network and react according to **Eq. 1** to form the carbonate salts in presence of unreacted sodium and calcium cations (Badar et al., 2014). This phenomenon is likely to occur in geopolymer matrices due to several factors, such as the porous network, the high alkalinity of the activation solution, and the weak bonding of alkali and alkaline cations within the geopolymer structure (Kani et al., 2012). Beneath the carbonate layer, samples cured in open containers exhibited small cracks due to a fast dehydration of the matrix, which caused shrinkage of the outermost layers (Kantarci et al., 2021). On the other hand, specimens cured in water-saturated sealed beakers behaved differently from the other two cases, coating with a film of water. This fact can be explained once again by observing **Eq. 1**: one molecule of water is produced for each of carbon dioxide which reacted with a hydroxyl ion. This water, which formed on the surface of the specimen, did not evaporate due to the saturated moisture condition, and dripped at the bottom of the container. This explanation would also justify the high pH measured in the solution at the bottom of the beaker, which exhibits values above 12, assessed with pH-testing stripes. Coherently, on the upper face stagnant droplets form, for they are not dragged by gravity.

Besides introducing modifications in the geopolymer appearance and microstructure, efflorescence lowers the pH of solutions in the pores, slowing down the geopolymerization reaction with negative effects on the mechanical properties (Criado et al., 2005). For this reason, it is important to monitor the compressive strengths of the specimens which underwent different curing conditions, since they experienced carbonation to different extents. The results are reported in **Figure 7** (right). It is immediate to notice that the humid environment provides the optimal curing condition, as higher compressive strength values are obtained for samples cured in water-saturated sealed containers. Exposure to a closed, humid environment may result in the opposite effect of direct exposure to air. While air exposure causes water evaporation, resulting in diffusion of the components towards the surface, the high moisture content outside the specimen allows the surface surface pores to hydrate, and such water would act as a barrier towards the permeation of CO_2 (Criado et al., 2005). Diffusion of gaseous and other mobile species is expected to occur mainly in the first hours of setting and curing, as the geopolymer gel has only partially reacted (Criado et al., 2005). For this reason, after the completion of the curing stage, i.e., once the geopolymer structure has been developed, the occurrence of further efflorescence should be impeded. As a further proof, it should be considered that samples

FIGURE 8
Geopolymeric specimens exposed to three different curing conditions: (left) open container; (centre) sealed container; (right) water-saturated sealed container.

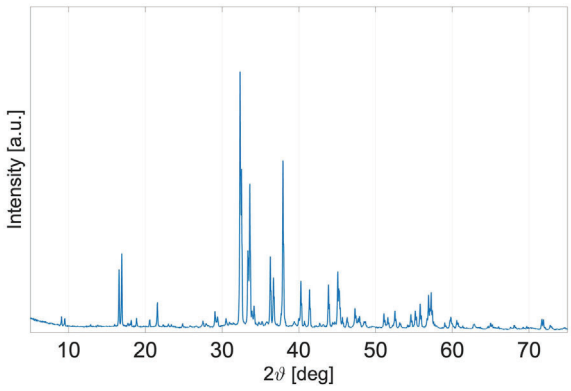

FIGURE 9
Diffraction pattern of the white polycrystalline material superficially growing on geopolymeric specimens exposed to air during curing.

re-exposed to air after water-saturated curing did not undergo surface carbonation, due to the complete crosslinking of the aluminosilicate networks. Moreover, a humid curing condition positively affects the mechanical resistance by preventing surface cracking due to shrinkage of the material (Longhi et al., 2022).

Leaching and immersion stability

Leaching experiments and post-immersion compression testing of formulations B, C, C-10, and C-20 were carried out to determine the release of matrix constituents and to investigate immersion-induced changes of the mechanical properties. The immersed specimens were continuously monitored by visual inspection and, after two weeks of immersion in water, no obvious disintegration, or any sign of cracking, was observed on any of the specimens. This suggests that the formed geopolymer proves resistant to immersion (Duxson et al., 2007; Ahmari and Zhang, 2013). **Figure 10** shows the released fractions of the main matrix constituents, i.e., sodium, aluminium, silicon, and calcium. The maximum released amount of each element is rather low, except for sodium which is about two orders of magnitude higher than the others. Besides higher mobility of sodium ions, this is due to the excess NaOH used to achieve sufficiently high alkalinity during the activation phase (Leong et al., 2016). As for silicon, aluminium, and calcium, less than 1% of the atoms for each element have leached from the matrix after more than 300 h of whole-body immersion. This further confirms that the aluminosilicate species have appropriately cross-linked, thus forming a promisingly durable geopolymeric matrix.

Among the two tested formulations (namely B and C), neither proved to be appreciably superior to the other in terms of retention of the four investigated elements. Formulation B seems to have the poorest confinement properties, at least for sodium, silicon, and calcium. However, the mass released is still more than comparable with that of the other geopolymers, which have overlapping curves in most cases. This result is in agreement with the literature. In fact, by increasing BFS content, the total porosity and pore volume decrease, hence both mechanical strength and permeability are reduced (Li and Liu, 2007; Provis and Bernal, 2014). The addition of SW in formulation C-10 and C-20 appreciably modifies, about a factor 2, the retention properties of the matrix.

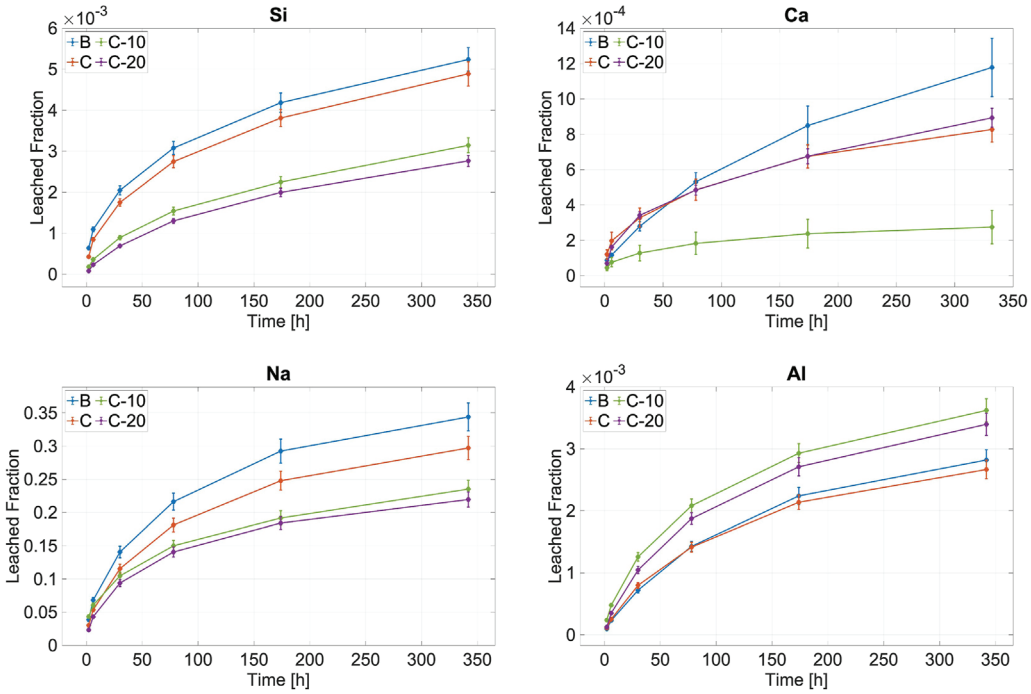

FIGURE 10
Cumulative release curves. The uncertainties bars on low values are within the marker size.

More accurate information can be deduced by comparing the leachability indices, reported in **Table 4** and computed in agreement with ANSI/ANS-16.1-2003 protocol over the whole leaching period (American Nuclear Society, 2003). The values of each element are similar between different formulations and within the uncertainty range. Coherently with **Figure 10**, the higher the leachability index the lower the released fraction. Sodium is the less confined element, as it is a highly mobile and weakly bound cation within the geopolymer structure (Kani et al., 2012; Sun and Vollpracht, 2020). This result agrees with the aforementioned excess of SH in the formulation. According to ANSI/ANS-16.1-2003 protocol (American Nuclear Society, 2003), for cumulative released fractions below 20 wt%, the leaching behaviour of the specimen approximates that of a semi-infinite medium, provided diffusion is the predominant phenomenon, and an expression exists to compute the diffusivity from the mass-transport equations. On the contrary, such approximation is not valid for released fractions above 20 wt%, and diffusivity values are derived from shape-specific solutions of the mass-transport equations. As a result, diffusion coefficients for sodium were computed in both ways, as leached fractions overcame the threshold value for the approximation of the leaching behaviour. Formulation B shows indices for the investigated elements close to those of formulation C, while the addition of SW, as anticipated before, induces a different lixiviation behaviour. For all the investigated elements,

TABLE 4 Leachability indices.

Formulation	Leachability indices			
	Na	Al	Si	Ca
B	7.06 ± 0.10	10.98 ± 0.37	11.71 ± 0.32	12.47 ± 0.28
C	7.27 ± 0.09	11.06 ± 0.29	11.71 ± 0.29	12.57 ± 0.44
C-10	7.55 ± 0.41	11.53 ± 0.11	11.37 ± 0.28	13.51 ± 0.59
C-20	7.60 ± 0.26	11.73 ± 0.30	11.49 ± 0.33	12.54 ± 0.32

the generally agreed requirement of 6 imposed by the reference WAC on leachability indices for cement-based matrices is well met (American Nuclear Society, 2003). These preliminary results suggest a promising durability of the novel matrices. Besides the preservation of the integrity of the monoliths, the zeolites endure to the geopolymerization reaction, as XRD analysis confirmed. For these reasons, no exceptions concerning the retention of contaminants, like Cs, Sr, and other fission and activation products are expected.

Compression tests downstream of immersion in water were performed on both the leached specimens and on the blank ones. The resulting strengths are reported in **Figure 11**. For formulations B, C, and C-20, immersion in water causes a deterioration of the mechanical properties of 15.9%, 9.5%, and 22.8% respectively, but it does not compromise the compliance with the requirement for cement-based matrices.

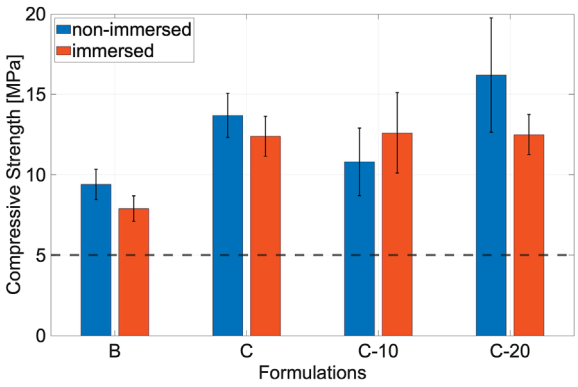

FIGURE 11
Compressive strength tests performed on leached and non-leached geopolymeric specimens. The dotted line represents the minimum value imposed by the WAC for cement-based matrices.

The reason may be the swelling of the material, caused by water absorption, which causes additional stress states in the material. A further explanation of the slight loss of mechanical resistance upon water immersion may be attributed to the partial dissolution of the hydrated gel phases (Lemougna et al., 2011; Firdous et al., 2018). In any case, on the other side, formulation C-10 shows an opposite behaviour. In this respect, it should be noted that the uncertainties of the two measurements for this geopolymer overlap, therefore it is not possible to ascertain whether water immersion increases its compressive strength. Large uncertainty bars in C-10 and C-20 samples are to be attributed to cavities and other casting defects in the samples. The preservation of the mechanical properties after immersion in water further proves the promising durability of these new matrices (Silva et al., 2012). In fact, both immersed and non-immersed samples showed compressive strengths far above the generally agreed WAC requirements for cement-based matrices.

Conclusion

The experimental work demonstrated the feasibility of treated RSOW encapsulation in novel geopolymer matrices synthesised from natural and recycled precursor materials. The use of natural zeolitic tuff as a substitute for MK and the recycling of industrial by-products foster the achievement of environmental and economic sustainability. Satisfactory crosslinking of the aluminosilicate species activated with solid NaOH was confirmed by microscopical and macroscopical investigations. The XRD analysis confirmed the activation of the precursors and the preservation of the zeolites during the geopolymerisation reactions, suggesting further investigation of their interactions with the contaminants present in real waste. Issues such as water evaporation and surface carbonation were coped with by identifying optimal curing conditions. By measuring setting time and workability of the fresh grouts, the logistical feasibility of the overall process was confirmed, fostering its scale-up. In addition, a representative surrogate waste was successfully encapsulated up to 20 wt% with no detriment to the mechanical and stability properties of the matrix. Preliminary experiments demonstrated the compliance with generally agreed waste acceptance criteria for cement-based matrices.

Future work aims at improving the properties of the matrix, increasing its performance, with a regard to the process characteristics for its production. Higher waste loading factors may be investigated, to reduce the overall volume of the final waste forms, and the encapsulation of other challenging radioactive waste may be addressed as well. Regarding the matrix formulation, optimisation work should be done, especially to further reduce its cost and the environmental footprint. For these reasons, but also to limit the phenomenon of surface carbonation, the sodium hydroxide content can probably be reduced to limit the phenomenon of surface carbonation together with the appropriate curing technique, reducing the environmental impact of the formulation. Water content should be optimized as well to face radiolysis-induced production of hydrogen. Up to now, only the energy-intensive MK has been replaced, but other materials could be used to replace FA and BFS as well, overcoming concerns about their worldwide availability. Finally, additional characterization of the precursors and of the matrix should be performed. A study of the exchange capacity of zeolites in tuff may confirm the improved cation retention capacity of this innovative geopolymeric formulation. The determination of the pore size distribution and, in general, a complete microstructural characterization may add additional information about the matrix durability.

Data availability statement

The original contributions presented in the study are included in the article/Supplementary Material, further inquiries can be directed to the corresponding author.

Author contributions

AS contributed to conceptualization, performed experimental activity, data processing, interpretation and curation, and drafted the manuscript. EMo contributed to conceptualization, supervision, data interpretation and curation, and manuscript review. GM, FG, and EMa supported data interpretation and contributed to review the manuscript. GG

and PL performed XRD analysis, interpreted the corresponding data, and contributed in drafting the manuscript. So did DV and DD for TGA. DC carried out macroscopic characterisations and reviewed the manuscript. HN supplied raw materials and dealt with data curation and manuscript review. MM provided resources and supervision. All the authors have contributed to the final proofreading and approval of the version for publication.

Funding

This work was conducted within H2020-PREDIS project, which has received funding support from the Euratom research and training programme 2019-2020 under grant agreement No. 945098.

Acknowledgments

The authors thank the KIPT (Ukraine) and Fertenia S.r.l. (Italy) for the provided materials (i.e., FA, BFS, and Zeolite Fertenia™ VT).

Conflict of interest

Author DC was employed by the company Nucleco S.p.A.

The remaining authors declare that the research was conducted in the absence of any commercial or financial relationships that could be construed as a potential conflict of interest.

The authors declare that this study received contribution from Fertenia S.r.l. which provided VT Zeolite Fertenia™ raw material. The company was not involved in the study design, collection, analysis, interpretation of data, the writing of this article or the decision to submit it for publication.

Publisher's note

References

Ahmari, S., and Zhang, L. (2013). Durability and leaching behavior of mine tailings-based geopolymer bricks. *Constr. Build. Mater.* 44, 743–750. doi:10.1016/j.conbuildmat.2013.03.075

Aliabdo, A. A., Abd Elmoaty, A. E. M., and Salem, H. A. (2016). Effect of cement addition, solution resting time and curing characteristics on fly ash based geopolymer concrete performance. *Constr. Build. Mater.* 123, 581–593. doi:10.1016/j.conbuildmat.2016.07.043

American Nuclear Society (2003). *Measurement of the leachability of solidified low-level radioactive wastes by a short-term test procedure* La Grange Park: American Nuclear Society. ANSI/ANS-16.1-2003.

Assi, L. N., Carter, K., Deaver, E., Anay, R., and Ziehl, P. (2018). Sustainable concrete: building a greener future. *J. Clean. Prod.* 198, 1641–1651. doi:10.1016/j.jclepro.2018.07.123

Assi, L. N., Carter, K., Deaver, E., and Ziehl, P. (2020). Review of availability of source materials for geopolymer/sustainable concrete. *J. Clean. Prod.* 263, 121477–121513. doi:10.1016/j.jclepro.2020.121477

Aydin, M. (2019). Renewable and non-renewable electricity consumptioneconomic growth nexus: Evidence from OECD countries. *Renew. Energy* 136, 599–606. doi:10.1016/j.renene.2019.01.008

Azam, A., Rafiq, M., Shafique, M., Zhang, H., Ateeq, M., and Yuan, J. (2021). Analyzing the relationship between economic growth and electricity consumption from renewable and non-renewable sources: Fresh evidence from newly industrialized countries. *Sustain. Energy Technol. Assess.* 44, 100991–100999. doi:10.1016/j.seta.2021.100991

Badar, M. S., Kupwade-Patil, K., Bernal, S. A., Provis, J. L., and Allouche, E. N. (2014). Corrosion of steel bars induced by accelerated carbonation in low and high calcium fly ash geopolymer concretes. *Constr. Build. Mater.* 61, 79–89. doi:10.1016/j.conbuildmat.2014.03.015

Baek, W., Ha, S., Hong, S., Kim, S., and Kim, Y. (2018). Cation exchange of cesium and cation selectivity of natural zeolites: Chabazite, stilbite, and heulandite. *Microporous Mesoporous Mater.* 264, 159–166. doi:10.1016/j.micromeso.2018.01.025

Bagheri, A., Nazari, A., Hajimohammadi, A., Sanjayan, J. G., Rajeev, P., Nikzad, M., et al. (2018). Microstructural study of environmentally friendly boroaluminosilicate geopolymers. *J. Clean. Prod.* 189, 805–812. doi:10.1016/j.jclepro.2018.04.034

Baykara, H., Cornejo, M. H., Murillo, R., Gavilanes, A., Paredes, C., and Elsen, J. (2017). Preparation, characterization and reaction kinetics of green cement: Ecuadorian natural mordenite-based geopolymers. *Mater. Struct.* 50, 188–212. doi:10.1617/s11527-017-1057-z

Bernal, S. A., Rodrguez, E. D., de Gutirrez, R. M., Gordillo, M., and Provis, J. L. (2011). Mechanical and thermal characterisation of geopolymers based on silicate-activated metakaolin/slag blends. *J. Mater. Sci.* 46, 5477–5486. doi:10.1007/s10853-011-5490-z

Bondar, D., Lynsdale, C. J., Milestone, N. B., Hassani, N., and Ramezanianpour, A. A. (2011). Effect of type, form, and dosage of activators on strength of alkali-activated natural pozzolans. *Cem. Concr. Compos.* 33, 251–260. doi:10.1016/j.cemconcomp.2010.10.021

British Standards Institution (2016). *Methods of testing cement-Part 3: Determination of setting times and soundness* London: BSI Standards Limited. BSI EN 196-3:2016.

British Standards Institution (2019). *Testing hardened concrete-Part 3: Compressive strength of test specimens* London: BSI Standards Limited. BSI EN 12390-3:2019.

British Standards Institution (2019). *Testing fresh concrete-Part 5: Flow table test* London: BSI Standards Limited. BSI EN 123505:2019.

Cantarel, V., Nouaille, F., Rooses, A., Lambertin, D., Poulesquen, A., and Frizon, F. (2015). Solidification/stabilisation of liquid oil waste in metakaolin-based geopolymer. *J. Nucl. Mater.* 464, 16–19. doi:10.1016/j.jnucmat.2015.04.036

Cappelletti, P., Rapisardo, G., de Gennaro, B., Colella, A., Langella, A., Graziano, S. F., et al. (2011). Immobilization of Cs and Sr in aluminosilicate matrices derived from natural zeolites. *J. Nucl. Mater.* 414, 451–457. doi:10.1016/j.jnucmat.2011.05.032

Castro, H. A., Luca, V., and Bianchi, H. L. (2017). Study of plasma off-gas treatment from spent ion exchange resin pyrolysis. *Environ. Sci. Pollut. Res.* 25, 21403–21410. doi:10.1007/s11356-017-8766-2

Chi, M. (2012). Effects of dosage of alkali-activated solution and curing conditions on the properties and durability of alkali-activated slag concrete. *Constr. Build. Mater.* 35, 240–245. doi:10.1016/j.conbuildmat.2012.04.005

Chindraprasirt, P., Jaturapitakkul, C., Chalee, W., and Rattanasak, U. (2009). Comparative study on the characteristics of fly ash and bottom ash geopolymers. *Waste Manag.* 29, 539–543. doi:10.1016/j.wasman.2008.06.023

Colella, C. (1996). Ion exchange equilibria in zeolite minerals. *Min. Depos.* 31, 554–562. doi:10.1007/bf00196136

Criado, M., Palomo, A., and Fernndez-Jimnez, A. (2005). Alkali activation of fly ashes. Part 1: Effect of curing conditions on the carbonation of the reaction products. *Fuel* 84, 2048–2054. doi:10.1016/j.fuel.2005.03.030

Davidovits, J. (1991). Geopolymers: Inorganic polymeric new materials. *J. Therm. Anal.* 37, 1633–1656.

Davidovits, J. (2018). "Geopolymers based on natural and synthetic metakaolin a critical review," in *Ceramic engineering and science proceedings*, 16, 201–214.

de Oliveira, L. B., de Azevedo, A. R. G., Marvila, M. T., Pereira, E. C., Fediuk, R., and Vieira, C. M. F. (2022). Durability of geopolymers with industrial waste. *Case Stud. Constr. Mater.* 16, 008399–e925. doi:10.1016/j.cscm.2021.e00839

Deir, E., Gebregziabiher, B. S., and Peethamparan, S. (2014). Influence of starting material on the early age hydration kinetics, microstructure and composition of binding gel in alkali activated binder systems. *Cem. Concr. Compos.* 48, 108–117. doi:10.1016/j.cemconcomp.2013.11.010

Diaz, E. I., Allouche, E. N., and Eklund, S. (2010). Factors affecting the suitability of fly ash as source material for geopolymers. *Fuel* 89, 992–996. doi:10.1016/j.fuel.2009.09.012

Djobo, J. N. Y., Tchadji, L. N., Tchakoute, H. K., Kenne, B. B. D., Elimbi, A., and Njopwouo, D. (2014). Synthesis of geopolymer composites from a mixture ofvolcanic scoria and metakaolin. *J. Asian Ceram. Soc.* 2, 387–398. doi:10.1016/j.jascer.2014.08.003

Djobo, J. N. Y., Elimbi, A., Tchakout, H. K., and Kumar, S. (2016). Reactivity of volcanic ash in alkaline medium, microstructural and strength characteristics of resulting geopolymers under different synthesis conditions. *J. Mater. Sci.* 51, 10301–10317. doi:10.1007/s10853-016-0257-1

Djobo, J. N. Y., Elimbi, A., Tchakout, H. K., and Kumar, S. (2016). Mechanical activation of volcanic ash for geopolymer synthesis: Effects on reaction kinetics, gel characteristics, physical and mechanical properties. *R. Soc. Chem. Adv.* 6, 39106–19117. doi:10.1039/c6ra03667h

Douiri, H., Kaddoussi, I., Baklouti, S., Arous, M., and Fakhfakh, Z. (2016). Water molecular dynamics of metakaolin and phosphoric acid-based geopolymers investigated by impedance spectroscopy and DSC/TGA. *J. Non-Cryst. Solids* 446, 95–101. doi:10.1016/j.jnoncrysol.2016.05.013

Dubois, M. A., Dozol, J. F., Nicotra, C., Serose, J., and Massiani, C. (1995). Pyrolysis and incineration of cationic and anionic ion-exchange resinsIdentification of volatile degradation compounds. *J. Anal. Appl. Pyrolysis* 31, 129–140. doi:10.1016/0165-2370(94)00817-k

Duxson, P., Provis, J. L., Lukey, G. C., Mallicoat, S. W., Kriven, W. M., and van Deventer, J. S. J. (2005). Understanding the relationship between geopolymer composition, microstructure and mechanical properties. *Colloids Surfaces A Physicochem. Eng. Aspects* 269, 47–58. doi:10.1016/j.colsurfa.2005.06.060

Duxson, P., Provis, J. L., Lukey, G. C., and van Deventer, J. S. J. (2007). The role of inorganic polymer technology in the development of 'green concrete. *Cem. Concr. Res.* 37, 1590–1597. doi:10.1016/j.cemconres.2007.08.018

Dyer, A., and Zubair, M. (1998). Ion-exchange in chabazite. *Microporous Mesoporous Mater.* 22, 135–150. doi:10.1016/s1387-1811(98)00069-9

Ekinci, E., Trkmen, ., Kantarci, F., and Karako, M. B. (2019). The improvement of mechanical, physical and durability characteristics of volcanic tuff based geopolymer concrete by using nano silica, micro silica and Styrene-Butadiene Latex additives at different ratios. *Constr. Build. Mater.* 201, 257–267. doi:10.1016/j.conbuildmat.2018.12.204

El Idrissi, A. C., Rozierre, E., Loukili, A., and Darson, S. (2018). Design of geopolymer grouts: The effects of water content and mineral precursor. *Eur. J. Environ. Civ. Eng.* 225, 628–649. doi:10.1080/19648189.2016.1214183

El-Eswed, B. I., Yousef, R. I., Alshaaer, M., Hamadneh, I., Al-Gharabli, S. I., and Khalili, F. (2015). Stabilization/solidification of heavy metals in kaolin/zeolite based geopolymers. *Int. J. Mineral Process.* 137, 34–42. doi:10.1016/j.minpro.2015.03.002

Ente Nazionale Italiano di Unificazione (2006). *Conditioned radioactive waste forms - qualification methods for the conditioning of Cathegory 2 waste forms* Milano: Ente Nazionale Italiano di Unificazione. UNI 11193:2006 (Document written in Italian).

European Commission (2022). PRE-DISposal management of radioactive waste. url: https://cordis.europa.eu/project/id/945098 (Accessed September 4th, 2022).

Fan, X. (2020). A brief introduction on the research status and future prospects on geopolymer concrete. *IOP Conf. Ser. Earth Environ. Sci.* 508, 012124–12210. doi:10.1088/1755-1315/508/1/012124

Fang, Y., and Kayali, O. (2013). The fate of water in fly ash-based geopolymers. *Constr. Build. Mater.* 39, 89–94. doi:10.1016/j.conbuildmat.2012.05.024

Firdous, R., Stephan, D., and Djobo, J. N. Y. (2018). Natural pozzolan based geopolymers: A review on mechanical, microstructural and durability characteristics. *Constr. Build. Mater.* 190, 1251–1263. doi:10.1016/j.conbuildmat.2018.09.191

Fournier, M., Massoni, N., and Hollebecque, J. F. (2020). In-Can vitrification of ash. *IOP Conf. Ser. Mater. Sci. Eng.* 818, 012005.

Ge, L., Wang, C., Hung, C., Liao, W., and Zhao, H. (2018). Assessment of strength development of slag cement stabilized kaolinite. *Constr. Build. Mater.* 184, 492–501. doi:10.1016/j.conbuildmat.2018.06.236

Geddes, D. A., Ke, X., Bernal, S. A., Hayes, M., and Provis, J. L. (2018). "Metakaolin-based geopolymers for nuclear waste encapsulation". in: *Calcined clays for sustainable concrete*. RILEM Bookseries. 16. 183–188.

Gralla, F., Abson, D. J., Mller, A. P., Lang, D. J., and von Wehrden, H. (2017). Energy transitions and national development indicators: A global review of nuclear energy production. *Renew. Sustain. Energy Rev.* 70, 1251–1265. doi:10.1016/j.rser.2016.12.026

Haddad, R. H., and Alshbuol, O. (2016). Production of geopolymer concrete using natural pozzolan: A parametric study. *Constr. Build. Mater.* 114, 699–707. doi:10.1016/j.conbuildmat.2016.04.011

Hajimohammadi, A., Ngo, T., Provis, J. L., Kim, T., and Vongsvivut, J. (2019). High strength/density ratio in a syntactic foam made from one-part mix geopolymer and cenospheres. *Compos. Part B Eng.* 173, 106908–106910. doi:10.1016/j.compositesb.2019.106908

Internatinal Atomic Energy Agency (1996). "Requirements and methods for low and intermediate level waste package acceptability," in *Technical documents series*, 864, 1–49.

International Atomic Energy Agency (2007). "Retrieval and conditioning of solid radioactive waste from old facilities," in *Technical reports series*, 456, 1–90.

International Atomic Energy Agency (2008). "Estimation of global inventories of radioactive waste and other radioactive materials," in *Technical documents series*, 1591, 1–31.

Ismail, I., Bernal, S. A., Provis, J. L., San Nicolas, R., Hamda, S., and van Deventer, J. S. J. (2014). Modification of phase evolution in alkali-activated blast furnace slag by the incorporation of fly ash. *Cem. Concr. Compos.* 45, 125–135. doi:10.1016/j.cemconcomp.2013.09.006

Istituto Superiore per la Protezione e la Ricerca Ambientale (1987). *Management of nuclear waste* Roma: Italian National Agency for New Technologies, Energy and Sustainable Economic Development. Technical Guide 26 (Document written in Italian).

Ji, Z., and Pei, Y. (2019). Bibliographic and visualized analysis of geopolymer research and its application in heavy metal immobilization: A review. *J. Environ. Manag.* 231, 256–267. doi:10.1016/j.jenvman.2018.10.041

Kani, E. N., Allahverdi, A., and Provis, J. L. (2012). Efflorescence control in geopolymer binders based on natural pozzolan. *Cem. Concr. Compos.* 34, 25–33. doi:10.1016/j.cemconcomp.2011.07.007

Kantarci, F., Trkmen, ., and Ekinci, E. (2019). Optimization of production parameters of geopolymer mortar and concrete: A comprehensive experimental study. *Constr. Build. Mater.* 228, 116770–116817. doi:10.1016/j.conbuildmat.2019.116770

Kantarci, F., Trkmen, ., and Ekinci, E. (2021). Influence of various factors on properties of geopolymer paste: A comparative study. *Struct. Concr.* 22, E315–E331. doi:10.1002/suco.201900400

Kouamo, H. T., Elimbi, A., Mbey, J. A., Ngally Sabouang, C. J., and Njopwouo, D. (2012). The effect of adding alumina-oxide to metakaolin and volcanic ash on geopolymer products: A comparative study. *Constr. Build. Mater.* 35, 960–969. doi:10.1016/j.conbuildmat.2012.04.023

Kumar, S., Kumar, R., and Mehrotra, S. P. (2010). Influence of granulated blast furnace slag on the reaction, structure and properties of fly ash based geopolymer. *J. Mater. Sci.* 45, 607–615. doi:10.1007/s10853-009-3934-5

Lee, W., Cheng, T., Ding, Y., Lin, K., Tsao, S., and Huang, C. (2019). Geopolymer technology for the solidification of simulated ion exchange resins with radionuclides. *J. Environ. Manag.* 235, 19–27. doi:10.1016/j.jenvman.2019.01.027

Lemont, F. (2012). Management of metal chlorides in high temperature processesApplication to the nuclear wastes treatment. *J. Hazard. Mater.* 213-214, 38–45. doi:10.1016/j.jhazmat.2012.01.038

Lemougna, P. N., MacKenzie, K. J. D., and Chinje Melo, U. F. (2011). Synthesis and thermal properties of inorganic polymers (geopolymers) for structural and refractory applications from volcanic ash. *Ceram. Int.* 378, 3011–3018. doi:10.1016/j.ceramint.2011.05.002

Leong, H. Y., Ong, D. E. L., Sanjayan, J. G., and Nazari, A. (2016). The effect of different Na_2O and K_2O ratios of alkali activator on compressive strength of fly ash based-geopolymer. *Constr. Build. Mater.* 106, 500–511. doi:10.1016/j.conbuildmat.2015.12.141

Li, Z., and Liu, S. (2007). Influence of slag as additive on compressive strength of fly ash-based geopolymer. *J. Mater. Civ. Eng.* 19, 470–474. doi:10.1061/(asce)0899-1561(2007)19:6(470)

Longhi, M. A., Rodrguez, E. D., Walkley, B., Eckhard, D., Zhang, Z., Provis, J. L., et al. (2022). Metakaolin-based geopolymers: Efflorescence and its effect on microstructure and mechanical properties. *Ceram. Int.* 48 , 2212–2229. doi:10.1016/j.ceramint.2021.09.313

Lopez-Solis, R., and Franois, J. L. (2018). The breed and burn nuclear reactor: A chronological, conceptual, and technological review. *Int. J. Energy Res.* 42, 953–965. doi:10.1002/er.3854

Luhar, I., and Luhar, S. (2022). A comprehensive review on fly ash-based geopolymer. *J. Compos. Sci.* 6, 219–259. doi:10.3390/jcs6080219

Martinez, L. G. (2022). Technological challenges to safe disposal of radioactive waste. url: https://www.iaea.org/newscenter/news/technological-challenges-safe-disposal-radioactive-waste. (Accessed July 21st, 2022).

Mozumder, R. A., Laskar, A. I., and Hussain, M. (2017). Empirical approach for strength prediction of geopolymer stabilized clayey soil using support vector machines. *Constr. Build. Mater.* 132, 412–424. doi:10.1016/j.conbuildmat.2016.12.012

Nath, P., and Sarker, P. K. (2014). Effect of GGBFS on setting, workability and early strength properties of fly ash geopolymer concrete cured in ambient condition. *Constr. Build. Mater.* 66, 163–171. doi:10.1016/j.conbuildmat.2014.05.080

Nath, S. K., Mukherjee, S. Maitra S., and Kumar, S. (2017). Kinetics study of geopolymerization of fly ash using isothermal conduction calorimetry. *J. Therm. Anal. Calorim.* 127, 1953–1961. doi:10.1007/s10973-016-5823-x

Niu, X., Elakneswaran, Y., Islam, C. R., Provis, J. L., and Sato, T. (2022). Adsorption behaviour of simulant radionuclide cations and anions in metakaolin-based geopolymer. *J. Hazard. Mater.* 429, 128373–128411. doi:10.1016/j.jhazmat.2022.128373

Pan, Z., Sanjayan, J. G., and Rangan, B. V. (2009). An investigation of the mechanisms for strength gain or loss of geopolymer mortar after exposure to elevated temperature. *J. Mater. Sci.* 44, 1873–1880. doi:10.1007/s10853-009-3243-z

Parthiban, D., Vijayan, D. S., Koda, E., Vaverkova, M. D., piechowicz, K., Osinski, P., et al. (2019). Role of industrial based precursors in the stabilization of weak soils with geopolymers. *Case Stud. Constr. Mater.* 16, 1–17.

Pasupathy, K., Berndt, M., Castel, A., Sanjayan, J., and Pathmanathan, R. (2016). Carbonation of a blended slag-fly ash geopolymer concrete in field conditions after 8 years. *Constr. Build. Mater.* 125, 661–669. doi:10.1016/j.conbuildmat.2016.08.078

Perera, F. (2018). Pollution from fossil-fuel combustion is the leading environmental threat to global pediatric health and equity: Solutions exist. *Int. J. Environ. Res. Public Health* 1516, 16–17. doi:10.3390/ijerph15010016

Phoo-ngernkham, T., Maegawa, A., Mishima, N., Hatanaka, S., and Chindaprasirt, P. (2015). Effects of sodium hydroxide and sodium silicate solutions on compressive and shear bond strengths of FAGBFS geopolymer. *Constr. Build. Mater.* 91, 1–8. doi:10.1016/j.conbuildmat.2015.05.001

Podolsky, Z., Liu, J., Dinh, H., Doh, J. H., Guerrieri, M., and Fragomeni, S. (2021). State of the art on the application of waste materials in geopolymer concrete. *Case Stud. Constr. Mater.* 15, 006377–e719. doi:10.1016/j.cscm.2021.e00637

Provis, J. L., and Bernal, S. A. (2014). Geopolymers and related alkali-activated materials. *Annu. Rev. Mater. Res.* 44, 299–327. doi:10.1146/annurev-matsci-070813-113515

Provis, J. L., Palomo, A., and Shi, C. (2015). Advances in understanding alkali-activated materials. *Cem. Concr. Res.* 78, 110–125. doi:10.1016/j.cemconres.2015.04.013

Qaidi, S. M. A., Tayeh, B. A., Isleem, H. F., de Azevedo, A. R. G., Ahmed, H. U., and Emad, W. (2022). Recycling of mine tailings for the geopolymer production: A systematic review. *Case Stud. Constr. Mater.* 16, 1–22.

Qaidi, S. M. A., Tayeh, B. A., Isleem, H. F., de Azevedo, A. R. G., Ahmed, H. U., and Emad, W. (2022). Sustainable utilization of red mud waste (bauxite residue) and slag for the production of geopolymer composites: A review. *Case Stud. Constr. Mater.* 16, 009944–e1028. doi:10.1016/j.cscm.2022.e00994

Rashad, A. M., and Zeedan, R. S. (2011). The effect of activator concentration on the residual strength of alkali-activated fly ash pastes subjected to thermal load. *Constr. Build. Mater.* 25, 3098–3107. doi:10.1016/j.conbuildmat.2010.12.044

Rattanasak, U., and Chindaprasirt, P. (2009). Influence of NaOH solution on the synthesis of fly ash geopolymer. *Miner. Eng.* 22, 1073–1078. doi:10.1016/j.mineng.2009.03.022

Reeb, C., Pierlot, C., Davy, C., and Lambertin, D. (2021). Incorporation of organic liquids into geopolymer materials - a review of processing, properties and applications. *Ceram. Int.* 47, 7369–7385. doi:10.1016/j.ceramint.2020.11.239

Rickard, W. D. A., Vickers, L., and van Riessen, A. (2013). Performance of fibre reinforced, low density metakaolin geopolymers under simulated fire conditions. *Appl. Clay Sci.* 73, 71–77. doi:10.1016/j.clay.2012.10.006

Scheithauer, D., Heschel, W., Meyer, B., and Krzack, S. (2017). Pyrolysis of undoped and multi-element doped ion exchange resins with regard to storage properties. *J. Anal. Appl. Pyrolysis* 124, 276–284. doi:10.1016/j.jaap.2017.01.024

Silva, I., Castro-Gomes, J. P., and Albuquerque, A. (2012). Effect of immersion in water partially alkali-activated materials obtained of tungsten mine waste mud. *Constr. Build. Mater.* 35, 117–124. doi:10.1016/j.conbuildmat.2012.02.069

Siyal, A. A., Shamsuddin, M. R., Khan, M. I., Rabat, N. E., Zulfiqar, M., Man, Z., et al. (2018). A review on geopolymers as emerging materials for the adsorption of heavy metals and dyes. *J. Environ. Manag.* 224, 327–339. doi:10.1016/j.jenvman.2018.07.046

Sun, Z., and Vollpracht, A. (2020). Leaching of monolithic geopolymer mortars. *Cem. Concr. Res.* 136, 106161–106212. doi:10.1016/j.cemconres.2020.106161

Walbrück, K., Maeting, F., Witzleben, S., and Stephan, D. (2020). Natural fiber-stabilized geopolymer FoamsA review. *Materials* 13, 3198–3225. doi:10.3390/ma13143198

Wang, J., and Wan, Z. (2015). Treatment and disposal of spent radioactive ion-exchange resins produced in the nuclear industry. *Prog. Nucl. Energy* 78, 47–55. doi:10.1016/j.pnucene.2014.08.003

Weng, L., and Sagoe-Crentsil, K. (2007). Dissolution processes, hydrolysis and condensation reactions during geopolymer synthesis: Part ILow Si/Al ratio systems. *J. Mater. Sci.* 42, 2997–3006. doi:10.1007/s10853-006-0820-2

Xie, F., Liu, C., and Wang, N. (2018). Threshold effects of new energy consumption transformation on economic growth. *Sustainability* 10, 4124–4214. doi:10.3390/su10114124

Xie, J., Wang, J., Rao, R., Wang, C., and Fang, C. (2019). Effects of combined usage of GGBS and fly ash on workability and mechanical properties of alkali activated geopolymer concrete with recycled aggregate. *Compos. Part B Eng.* 164, 179–190. doi:10.1016/j.compositesb.2018.11.067

Yao, X., Zhang, Z., Zhua, H., and Chena, Y. (2009). Geopolymerization process of alkalimetakaolinite characterized by isothermal calorimetry. *Thermochim. Acta* 493, 49–54. doi:10.1016/j.tca.2009.04.002

Ye, H., and Radliska, A. (2017). Carbonation-induced volume change in alkali-activated slag. *Constr. Build. Mater.* 144, 635–644. doi:10.1016/j.conbuildmat.2017.03.238

Yip, C. K., Lukey, G. C., and van Deventer, J. S. J. (2005). The coexistence of geopolymeric gel and calcium silicate hydrate at the early stage of alkaline activation. *Cem. Concr. Res.* 35, 1688–1697. doi:10.1016/j.cemconres.2004.10.042

Zakharova, K. P., and Masanov, O. L. (2000). Bituminization of liquid radioactive wastes. Safety assessment and operating experience. *At. Energy* 89, 646–649. doi:10.1023/a:1011399408845

Zhang, X., Gu, P., and Liu, Y. (2009). Decontamination of radioactive wastewater: State of the art and challenges forward. *Chemosphere* 215, 543–553. doi:10.1016/j.chemosphere.2018.10.029